Lattice gas description of pyrochlore and checkerboard antiferromagnets in a strong magnetic field

M. E. Zhitomirsky

Commissariat à l'Energie Atomique, DSM/DRFMC/SPSMS, 38054 Grenoble, France

Hirokazu Tsunetsugu

Institute for Solid State Physics, University of Tokyo, Kashiwa, Chiba 277-8581, Japan
(Dated: 08 March, 2007)

Quantum Heisenberg antiferromagnets on pyrochlore and checkerboard lattices in a strong external magnetic field are mapped onto hard-core lattice gases with an extended exclusion region. The effective models are studied by the exchange Monte Carlo simulations and by the transfer matrix method. The transition point and the critical exponents are obtained numerically for a square-lattice gas of particles with the second-neighbor exclusion, which describes a checkerboard antiferromagnet. The exact structure of the magnon crystal state is determined for a pyrochlore antiferromagnet.

I. INTRODUCTION

A characteristic feature of geometrically frustrated spin models is an infinite degeneracy of the classical ground state. Such a degeneracy may be lifted by quantum or thermal fluctuations via the 'order from disorder' effect.[1,2,3] A closely related property is emergence of small energy scales, which are described by the effective Hamiltonians acting in the subspace of nearly degenerate low-energy quantum states. To date, several types of effective models have been developed for frustrated antiferromagnets in different regimes. The first example is a celebrated quantum dimer model introduced phenomenologically by Rokhsar and Kivelson to describe a magnetically disordered resonating valence bond phase of $S = 1/2$ antiferromagnets.[4] Recently, effective quantum dimer models have been derived for several realistic spin Hamiltonians in zero and in a finite magnetic field.[5,6,7] The second example is the effective Hamiltonian for the collinear states, which applies to a semiclassical ($S \gg 1$) pyrochlore antiferromagnet in zero magnetic field.[8] The third type of effective models describes geometrically frustrated magnets at high magnetic fields.[9,10,11,12] These are the so called lattice-gas models considered further in the present work.

Previously, the effective lattice-gas models have been derived and discussed for the sawtooth chain and a kagomé antiferromagnet.[9,10,11] These two quantum antiferromagnets are mapped onto lattice gases of hard-core classical particles with the nearest-neighbor exclusion on a one-dimensional chain and a triangular lattice, which are respectively called the hard-dimer and the hard-hexagon model. In both cases, the thermodynamics of the effective models has been calculated exactly.[13] In the present article, we shall focus on the high-field behavior of quantum antiferromagnets on two- and three-dimensional pyrochlore lattices. The corresponding effective models do not allow exact solution for their thermodynamic properties, therefore, we shall study them via a
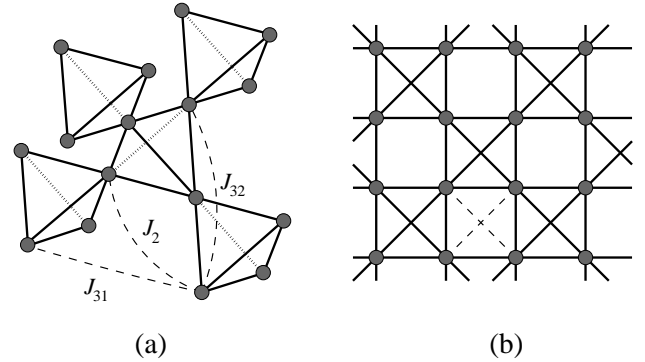

FIG. 1: Pyrochlore lattice of corner-sharing tetrahedra (a) and its two-dimensional analog, checkerboard lattice (b). Solid lines show the nearest-neighbor bonds of strength J. Dashed lines indicate possible further neighbor exchanges.

combination of numerical techniques.

The pyrochlore and the checkerboard lattices (Fig. 1) consist of 3D and 2D networks of corner-sharing tetrahedra (four-spin blocks). For the most part of the present work, we disregard weak further neighbor exchanges and consider the nearest-neighbor Heisenberg model with an arbitrary spin S in an external magnetic field:

$$\hat{\mathcal{H}} = J \sum_{\langle ij \rangle} \mathbf{S}_i \cdot \mathbf{S}_j - \mathbf{H} \cdot \sum_i \mathbf{S}_i \ . \tag{1}$$

Above the saturation field H_s the ground state of a Heisenberg antiferromagnet is a fully polarized vacuum $|0\rangle = |\uparrow\uparrow\uparrow ...\rangle$, where all spins are in a state with the maximum possible value of $S_i^z = S$. The low-lying excitations are single spin flips $|i\rangle = S_i^-|0\rangle$, whose dispersion can be straightforwardly calculated. The characteristic feature of many geometrically frustrated models including the two considered models is presence of the low-energy branch of localized magnons with the energy $\varepsilon_0 = H - H_s$.[14,15,16,17,18] The details for the two discussed

models are presented in the subsequent sections.

Localized nature of magnons from the lowest branch allows to construct a subclass of exact multimagnon states:[15] a quantum state with m localized magnons (m-LMs) occupying spatially separated regions of the lattice, which are not directly connected by the exchange bonds, is an exact eigenstate of the quantum Hamiltonian (1) and its energy is given by $m\varepsilon_0$. It has been proven exactly that isolated LM states correspond to the lowest energy states in every magnetization subsector.[10,16] In addition, the renormalization arguments suggest that delocalized (propagating) states are separated by a finite gap from LMs.[9,10] Hence, at low temperatures the partition function of a quantum frustrated antiferromagnet in the vicinity of the saturation field is determined entirely by LMs:

$$\mathcal{Z} = \sum_{m=0}^{N_{\max}} w(m,N)\, e^{m\mu/T} \;, \quad \mu = H_s - H \;, \qquad (2)$$

with $z = e^{\mu/T}$ being the activity. Combinatorial factors $w(m,N)$ denote a number of linearly independent m-LM states, while $N_{\max}$ is the maximal number of LMs for a lattice with N sites ($N \to \infty$). Mapping to a lattice gas of hard-core objects is used as an *approximate* way to calculate $w(m,N)$ and $\mathcal{Z}$. The general consequence of Eq. (2) is the following scaling of the total entropy: $\mathcal{S} = f[(H - H_s)/T]$. At $H = H_s$ the entropy is temperature independent and, consequently, even at $T = 0$ a frustrated quantum antiferromagnet has a finite macroscopic entropy, which is determined purely by the lattice geometry. The quantum order from disorder mechanism becomes ineffective for this special value of applied field due to the localized nature of (exact) quantum states with zero energy. In Secs. II and III we describe derivation of lattice gas mapping and obtain conclusions separately for the checkerboard and the pyrochlore antiferromagnet. Role of extra exchanges beyond the nearest-neighbor pairs, see Fig. 1, is briefly discussed in Sec. IV.

II. CHECKERBOARD ANTIFERROMAGNET

A. Localized magnon states

A checkerboard lattice contains two spins in the primitive unit cell. The corresponding Bravais lattice is formed by elementary translations on $\mathbf{a}_1 = (1,1)$ and $\mathbf{a}_2 = (-1,1)$ and has a square shape. In the saturated phase at high fields, the one-magnon spectrum has, accordingly, two branches:

$$\omega_{1\mathbf{k}} = H - 8JS \;, \qquad \omega_{2\mathbf{k}} = H - 4JS(1 - \gamma_{\mathbf{k}}) \;, \qquad (3)$$

where $\gamma_{\mathbf{k}} = \cos k_x \cos k_y$. The saturation field $H_s = 8JS$ corresponds to the vanishing energy of magnons from the lowest dispersionless branch $\omega_{1\mathbf{k}}$. Localization of excitations from the lowest branch is determined by the lattice
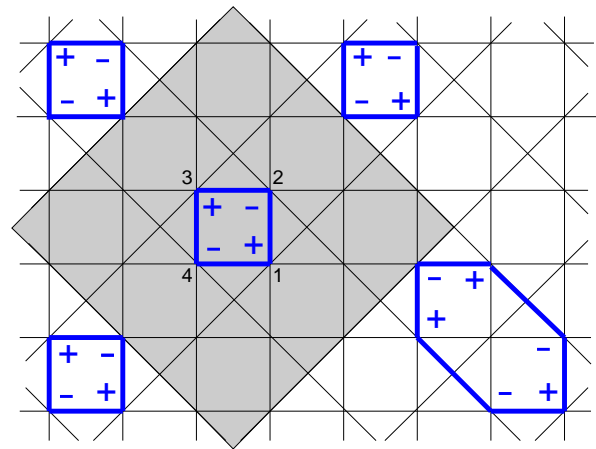

FIG. 2: (color online). Localized magnons on a checkerboard lattice. Thick lines indicate positions of one-magnon states with corresponding phases shown by $+$ and $-$. The shaded area shows excluded volume around a central square-void state, which has to be respected for construction of multiparticle states. Four LMs in the upper-left part satisfy a close-packed condition (see the text).

topology. A simple localized state can be constructed as a spin-flip trapped on a square void of a checkerboard lattice:

$$|\varphi_i\rangle = \frac{1}{\sqrt{8S}} \sum_{n=1}^{4} (-1)^{n-1} S_{ni}^- |0\rangle \;, \qquad (4)$$

where the numbering of sites goes counterclockwise starting from the lowest right corner, see Fig. 2. The probability to find spin-flip on a site adjacent to the void vanishes due to the destructive interference. This property crucially depends on equal strength of all bonds of the checkerboard lattice.

A linear combination of two square-void states sharing one vertex encompasses two square voids and so on, see Fig. 2. An arbitrary 1-LM state can be constructed by drawing a closed graph on the original lattice, which passes through two vertices of every crossed four-site block, and assigning $+$ and $-$ signs in alternate order for a spin-flip propagating around it. The smallest square-void states play an important role by forming a complete nonorthogonal basis in the subspace of dispersionless one-magnon states.[10] The multi-particle LM states are, then, constructed by respecting topology of the exchange bonds: LMs cannot occupy square voids, which are contiguous to the same crossed square as shown in Fig. 2 by shaded area.

There is an upper limit on the density of isolated localized magnons. For a checkerboard lattice, a close-packed structure is constructed by putting LMs on every second square void in horizontal rows with an alternating shift between the rows, see the left part in Fig. 2. This pattern corresponds to a magnon crystal, which breaks translational symmetry and has the density of LMs equal

to $n_0 = N_{\max}/N = 1/8$. The breaking of the translational symmetry is, however, incomplete: *diagonal* rows of LMs can freely slide without affecting magnons in adjacent rows. The degeneracy of the magnon crystal state is $N_{\mathrm{deg}} \sim 2^{L+1}$, where L is a linear size of the system, see also Sec. IIc. Note, that the magnon crystal for a quantum kagomé antiferromagnet is only three-fold degenerate. In that case there is a well-defined finite temperature transition associated with the translational symmetry breaking.

The purpose of the present study is to investigate the low-temperature behavior of the checkerboard antiferromagnet and nature of a phase transition into the magnon crystal state. In order to proceed, we map a quantum checkerboard antiferromagnet in the vicinity of the saturation onto a gas of hard-core particles. Such an effective model is defined on a $\sqrt{2} \times \sqrt{2}$ square lattice formed by centers of square voids of the original checkerboard lattice. The dual square lattice is rotated by $45°$ and contains $N/2$ sites. Localized magnons are represented by hard-core classical particles obeying the nearest- and the next-nearest neighbor exclusion principle. Below, we call them 'hard-polygon states.' One such polygon for a checkerboard lattice is shown in Fig. 2 by a shaded square. In reality a state with two localized magnons occupying adjacent sites is separated by only a finite gap from the low-lying LM states. An estimate of such gap for a kagomé lattice antiferromagnet is given in Ref. 9. In the following only $T \to 0$ regime is considered, where contribution of such higher energy states can be neglected.

B. Topological classes of localized magnons

The hard-polygon states being linearly independent[19] do not exhaust all possible localized magnon states. The missing 'defect' states belong to different topological classes of LMs.[9,10] Let us consider an infinite plane with open boundary conditions, which has topology of a sphere without the North pole. As was explained before, one-particle localized states correspond to closed lines. Successive expansion of the wave-function of a one-magnon state in terms of basis plaquette states can be represented as a gradual deformation of a long loop with subsequent contraction into a point (center of the last plaquette). Two closed loops for a 2-LM state may be either contractible to two distinct points on a plane or lie inside each other and, hence, be contractible into a single point, see Figs. 3a and 3b. In the first case the two magnon state belongs to a subset of two-particle hard-polygon states, whereas in the second case an expansion in the hard-polygon states is impossible. The two-magnon states shown in Figs. 3a and 3b are, therefore, *linearly independent*.

Situation is somewhat different for a cluster with periodic boundary conditions, which has a torus topology. In that case one can continuously deform the outer line in Fig. 3b, split it into two loops with finite winding around
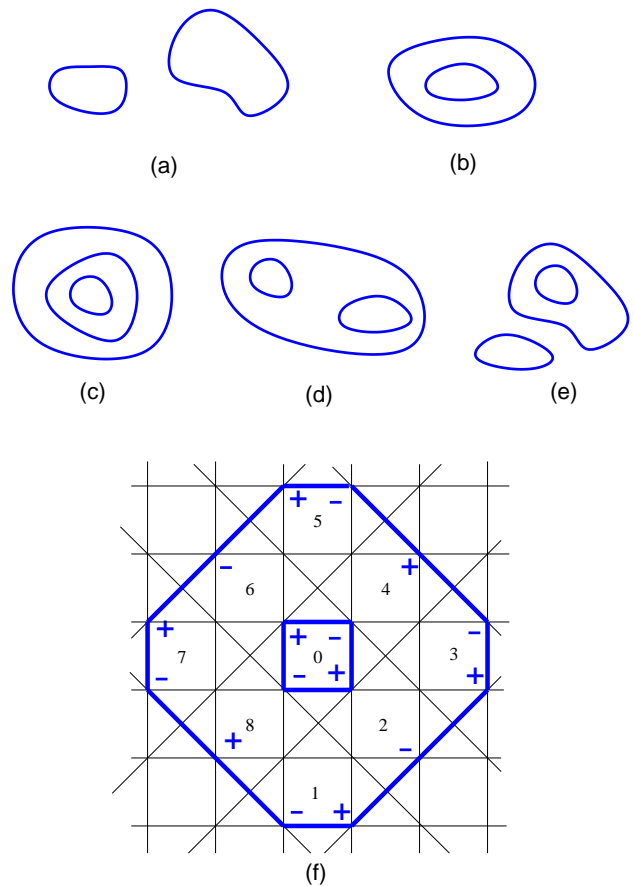

FIG. 3: (color online). Examples of topologically different states of localized magnons: 2-magnon subsector (a) and (b); 3-magnon subsector (c)–(e); (f) shows an elementary defect state from the class (b).

the torus, move them around and close again into one contour on the opposite side such that the two-magnon state in Fig. 3b transforms into a state of type Fig. 3a. The linear dependence of two-magnon states in Figs. 3a and 3b for the torus topology is explained by presence in this case of one linear relation between 1-LM square-void (hexagon) states.[10] Still, there are additional 2-LM states in this topology, which are constructed by putting one or two LMs on contours with nontrivial winding around the torus. Topologically nontrivial classes of LM states in the three-magnon subsector for a lattice with open boundary conditions are shown in Figs. 3c–e. For periodic boundary conditions the state in Fig. 3c becomes topologically equivalent to the state in Fig. 3e, while the state Fig. 3d can be transformed into the hard-polygon state. The macroscopic limit, however, does not depend on the boundary conditions. Equivalence of the two approaches in the $N \to \infty$ limit is recovered by observing that the largest number of topologically nontrivial LM states in n-magnon subsectors with $n > 2$ is given by states of the type shown in Fig. 3e, which are present for both choices of boundary conditions. Disentanglement of

two, three, etc. enclosed loops in the torus topology is impossible once other LMs are present. On the other hand, the contribution from closed loops with a nontrivial winding around the torus corresponds in the thermodynamic limit only to a surface effect.

Topological origin of the additional localized magnon states determines their presence for all two-dimensional frustrated models including antiferromagnets on kagomé, checkerboard, and star lattices. There are no such states in one-dimensional models as, for example, the sawtooth chain, where the hard-particle representation is asymptotically exact.[9,10] In order to estimate the contribution of additional LMs, one has to define the basis states in the topologically nontrivial classes. The elementary defect state in the topological class of Fig. 3b is shown in Fig. 3f (open boundary conditions are assumed). Its wave-function is given by

$$|2\text{-defect}\rangle \simeq \Big(\sum_{i=1}^{8}(-1)^{i-1}|\varphi_i\rangle + |\varphi_0\rangle\Big)|\varphi_0\rangle , \qquad (5)$$

where the numbering of plaquette states follows Fig. 3f. This wave-function includes two LMs on adjacent voids and on the central plaquette and violates, therefore, the hard-polygon constraint. The two-magnon states (5) residing on different central squares are linearly independent and form a nonorthogonal basis in the subspace of topologically nontrivial graphs of Fig. 3b. The 2-LM defect state (5) can be identified with a new classical particle, which has energy $2\varepsilon_0$ and a longer-range repulsion. Such a mapping suggests that the topologically nontrivial states yield an additional macroscopic contribution to the partition function $\mathcal{Z}$. Their share is, however, suppressed compared to the hard-polygon contribution by a large entropic factor: region occupied by the basis two-magnon state, Fig. 3f, can be occupied by 16 different 2-LM states residing on small empty squares. In addition, by counting the total number of excluded square voids we conclude that the states (5) do not contribute appreciably to the magnetization subsectors with the average density of LMs larger than $n \gtrsim 2/(25\cdot 2) = 0.04$.[10] Consequently, their role at high densities, *e.g.*, in the vicinity of the transition into a magnon crystal state is strongly suppressed. Alternatively, the lattice gas mapping can be improved by including extra types of particles, which describe LMs from different topological classes. Below we consider the simplest version of the lattice gas mapping with only one type of particles.

C. Effective lattice-gas model

Two-dimensional lattice gas models were originally suggested to study atomic adsorption on various substrates.[20,21,22,23,24,25,26,27,28] They also describe low-T behavior of Ising antiferromagnets in a longitudinal field.[24,29,30] Despite the long-lasting interest there are only few well-established facts for a square lattice

TABLE I: The entropy per site $\mathcal{S}$ and the density n of a hard-square lattice gas with second-neighbor exclusion at $\mu = 0$ obtained from the transfer matrix calculation on a semi-infinite strip $M \times \infty$.

M	$\mathcal{S} = \dfrac{\ln \lambda_1}{M}$	n
8	0.294795	0.13713
10	0.294671	0.13686
12	0.294647	0.13679
14	0.294642	0.13677

gas with the nearest- and the next-nearest-neighbor exclusion. It is generally accepted that this model exhibits a continuous phase transition into a partially ordered (2×1) phase.[21,25] This phase transition belongs to the universality class of an XY model with a four-fold anisotropy,[23] which is a special case of a more general $Z(4)$ discrete planar model.[31,32,33] Depending on the values of two coupling constants the $Z(4)$ model exhibits either two Ising-like transitions between a paramagnetic and an ordered state or a single critical point,[32] which has nonuniversal critical exponents.[34] Estimates for the transition point of a hard-square lattice gas with the second-neighbor repulsion vary from $\ln z_c = (\mu/T)_c = 5.3$ in the early work[21] to $\ln z_c = 4.7$ in the later study.[25] There is even less certainty about values of the critical exponents. The entropy of the system at $\mu = 0$, which is an interesting property of a quantum antiferromagnet, has not been investigated in the context of previous applications.

First, we investigate numerically the entropy of the lattice gas model at zero chemical potential. This can be done by the transfer matrix method and Monte Carlo simulations. The former method has been a standard technique since the early studies of two-dimensional lattice gas models.[21,25,29] In this scheme a two dimensional lattice is represented by a semi-infinite strip of width M and the thermodynamic properties are derived from the largest eigenvalue λ_1 of the transfer matrix. In particular, the entropy normalized per one site is equal to $\mathcal{S} = (\ln \lambda_1)/M$. The actual calculations become quite simple for $\mu = 0$, when the elements of the transfer matrix take only values 0 or 1. The results for a few values of M are presented in table I. The convergence is very rapid and already the $M = 10$ strip gives four significant digits for the entropy.

To determine entropy from Monte Carlo (MC) simulations we adopt the following procedure. The standard Metropolis algorithm is used for gradual annealing from the low-activity regime $\ln z = -20$, where the density of particles is vanishingly small and $\mathcal{S} = 0$, to the point $\ln z = 0$. The step for the chemical potential is chosen to be small enough $\Delta(\ln z) = 0.05$. At every value of μ 10^4 MC steps (lattice sweeps) are performed for equilibration and after that 10^5 MC steps are used to measure $(\partial \mathcal{S}/\partial \mu)_T$, which is calculated from the cumulant of the
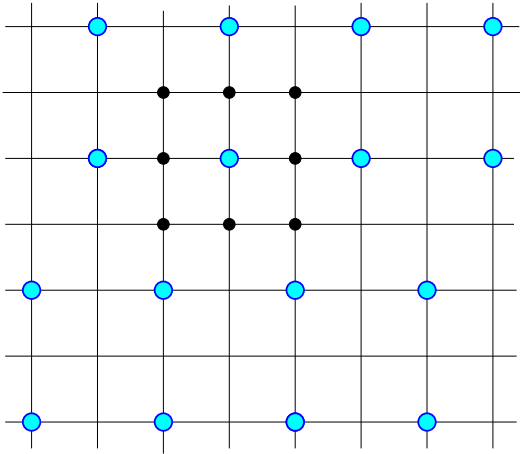
FIG. 4: (color online). Effective lattice gas model for a checkerboard antiferromagnet. The dual square lattice is 45° rotated compared to the original checkerboard lattice in Fig. 2 and has twice less sites. Hard particles are shown by large light circles; small dark circles indicate the excluded sites around one particle. The presented close-packed structure with half-filled rows randomly shifted in the horizontal direction has a nonzero Fourier harmonic at $\mathbf{Q}_1 = (0, \pi)$.
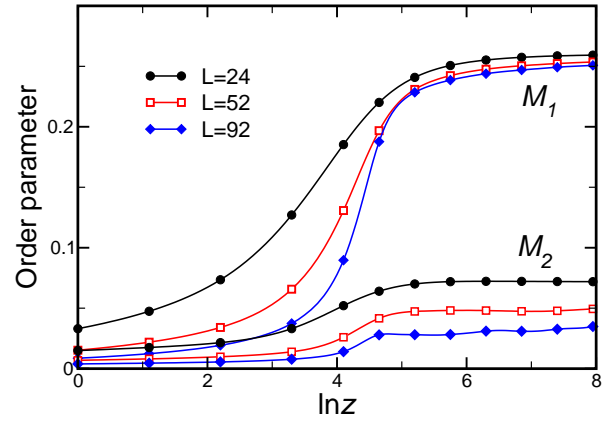

FIG. 5: (color online). Dependence of the two order parameters Eq. (7) on logarithm of the fugacity $\ln z = \mu/T$ for three system sizes.

energy E and the number of particles $\mathcal{N}$:

$$\left(\frac{\partial \mathcal{S}}{\partial \mu}\right)_T = \frac{1}{T^2}(\langle E\mathcal{N}\rangle - \langle E\rangle\langle\mathcal{N}\rangle) . \tag{6}$$

In our case $E = -\mu\mathcal{N}$ and the cumulant in Eq. (6) is proportional to the variance of the total number of particles. The error bars are estimated by performing up to 100 independent runs with different sequences of random numbers. Afterwords, the data for $(\partial \mathcal{S}/\partial \mu)_T$ are numerically integrated to find $\mathcal{S}|_{\mu=0}$. Simulations have been performed on square clusters with periodic boundary conditions and $N = L^2$ sites, $L = 16, 32$, and 64. The obtained results agree with each other within numerical accuracy and yield $\mathcal{S} = 0.2946(1)$ for the entropy per site and $n = 0.13676(1)$ for the average density of particles. The found values are in good correspondence with the transfer-matrix results included in table I confirming the accuracy of both methods. The particle density at $\mu = 0$ is quite substantial and only two times smaller than the density of the close-packed structure $n_0 = 0.25$.

Once the chemical potential further increases ($z > 1$) more and more particles become condensed. Eventually the lattice gas transforms into an ordered close-packed structure. The order parameter of such a crystalline state are certain Fourier harmonic(s) of the particle density, $n_\mathbf{q} = (1/N)\sum_i n_i e^{-i\mathbf{q}\mathbf{r}_i}$. A close-packed structure with half-filled rows, which are randomly shifted in the x-direction has a nonzero harmonic at $\mathbf{Q}_1 = (0, \pi)$ with $n_{\mathbf{Q}_1} = 1/4$, see Fig. 4. A similar state with random shifts of columns along the y direction is described by $\mathbf{Q}_2 = (\pi, 0)$ and $n_{\mathbf{Q}_2} = 1/4$. These two phases are called (2×1) states in a standard nomenclature adopted for lat-

tice gas models.[26] A fully symmetric structure with all rows (columns) in phase with each other has equal amplitudes $n_{\mathbf{Q}_i} = 1/4$ for the three wave-vectors $\mathbf{Q}_1$, $\mathbf{Q}_2$, and $\mathbf{Q}_3 = (\pi, \pi)$ and is called a (2×2) state. The wave-vectors $\mathbf{Q}_1$ and $\mathbf{Q}_2$ belong to the same irreducible representation. Consequently, we consider two order parameters:

$$M_1 = (n_{\mathbf{Q}_1}^2 + n_{\mathbf{Q}_2}^2)^{1/2} , \quad M_2 = |n_{\mathbf{Q}_3}| . \tag{7}$$

The infinitely degenerate close-packed structure for a square-lattice gas with the second-neighbor exclusion leads to equilibration problems in simple MC simulations. This was evident since the early MC study of a frustrated Ising antiferromagnet,[24] which investigated clusters up to only 40^2 sites using a single spin-flip relaxation method. We employ instead an exchange MC algorithm proposed some time ago to tackle systems with extremely long relaxation times, as, for example, spin glasses.[35] With this modification we have been able to study clusters with up to 120^2 sites. To ensure a substantial replica exchange rate ~ 0.7–0.9, we have used 120 replicas in the range $0 \le \ln z \le 8$ for all system sizes. The simulation runs included 10^5 exchange MC steps for equilibration and up to 10^7 MC steps for measurements. Statistical errors were estimated from bining the MC series for each value of z.

The specific heat exhibits a broad and rounded maximum near to $\ln z \sim 4.4$. The height of the peak grows very slowly with increasing L, such that a preliminary determination of the transition point is impossible from the specific heat data. The ensemble averages of the two order parameters $\langle M_1\rangle$ and $\langle M_2\rangle$ are shown in Fig. 5. The square of the second order parameter $\langle M_2^2\rangle$ goes down to zero as $1/N$ with the system size, whereas $\langle M_1\rangle$ scales to a finite constant at $\ln z \ge 5$. The limiting value for the largest cluster is very close $1/4$ in accordance with the previous analysis for the (2×1) type of ordering. The precise location of the transition point is obtained by measuring the Binder cumulant $U_4 = \langle M_1^4\rangle/\langle M_1^2\rangle^2$. Its dependence on z is presented in Fig. 6. The tran-
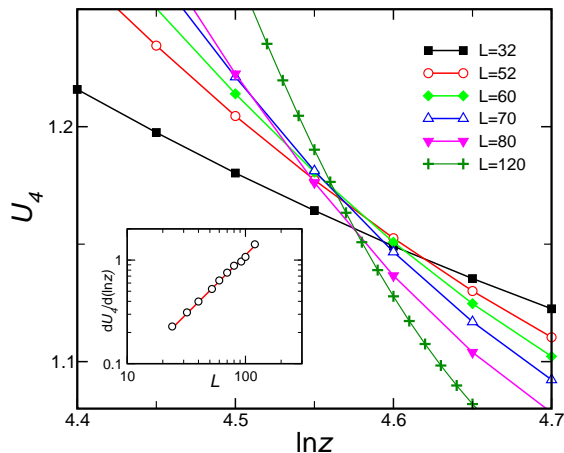
FIG. 6: (color online). Binder cumulant U_4 as a function of $\ln z = \mu/T$ for different cluster sizes L. The inset shows scaling of the derivative $dU_4/d(\ln z)$ at the transition point $\ln z_c = 4.56$ versus L.

sition point can be estimated from the crossing points of Binder cumulants for different clusters.[36] This yields $\ln z_c = 4.56 \pm 0.02$ for the critical activity. The density of particles at the transition point is $n_c = 0.2325(3)$.

In principle, the measurement of $M_1 \neq 0$ cannot discriminate between a single-k structure corresponding to the (2×1) order and a double-k structure with two nonzero Fourier harmonics $n_{\mathbf{Q}_1}, n_{\mathbf{Q}_2} \neq 0$. The two structures can be distinguished with the help of an order parameter, which probes breaking of the C_4 rotational symmetry:

$$\Delta = \frac{1}{N} \sum_i n_i(n_{i+2\mathbf{x}} - n_{i+2\mathbf{y}}) . \tag{8}$$

The order parameter Δ vanishes for the (2×2) state and all other states symmetric under 90° rotations, whereas it has a finite value in the (2×1) phase. We have calculated $\langle |\Delta(z)| \rangle$ by MC simulations and found that at $\ln z > 5$ within statistical errors it reaches a finite value: $\langle |\Delta| \rangle = 1/8$. This not only demonstrates an absence of the tetragonal symmetry in the ordered state, but also proves *random* shifts of half-filled rows (columns). For example, if shifts occur in a regular alternating order, than one would find $\langle |\Delta| \rangle = 1/4$, which is definitely excluded by our Monte Carlo results.

In order to determine the critical exponents, we performed finite-size scaling analysis of various thermodynamic quantities measured at the estimated critical point $\ln z_c$. The correlation length exponent ν is extracted from the behavior of the derivative of the Binder cumulant $dU_4/d(\ln z) \sim L^{1/\nu}$ at $z = z_c$. The fitting shown in the inset of Fig. 6 yields $1/\nu = 1.16 \pm 0.02$. The order parameter at criticality scales as $M(z_c) \sim L^{-\beta/\mu}$. A fit for a few largest L gives $\beta/\nu = 0.15(1)$. As a result, we obtain the following estimates $\nu = 0.86(2)$ and $\beta = 0.13(1)$. The largest clusters employed in the present study are

still not sufficient to independently extract the critical exponent α, presumably because of a large regular contribution to the specific heat compared to a universal singular part. The obtained values for β and ν place a hard-square gas with the second-neighbor exclusion on a line of critical points of the $Z(4)$ model between the Potts model, which has $\beta = 1/12$ and $\nu = 2/3$,[33] and the vector Potts model, which belongs to the Ising universality class with $\beta = 1/8$ and $\nu = 1$.[31] Our result for $\ln z_c$ coincides within the error bars with the corresponding value from the recent independent MC study of the same model,[37] though we do not share its claim of the Ising universality class for the transition.

Properties of a quantum spin-1/2 checkerboard antiferromagnet in the vicinity of the saturation field are obtained from the above results by a straightforward rescaling to the number of sites of checkerboard lattice, which is twice larger than the number of sites for the lattice gas. At $H = H_s$, the entropy and the magnetization normalized per one site have universal T-independent values:

$$\mathcal{S}_s = 0.1473 , \qquad M_s = 0.4316 . \tag{9}$$

Note, that the entropy of a checkerboard antiferromagnet is 30% larger than the corresponding result for a kagomé antiferromagnet.[9] The transition field into the magnon crystal phase is given by

$$H_c(T) = H_s - T \ln z_c = 4J - 4.56T . \tag{10}$$

Let us emphasize again that the entropy found within the lattice-gas (hard-polygon) description of LMs is only approximate. Localized magnons from different topological classes will increase the above value of $\mathcal{S}_s$. Such corrections should not be very large in view of a large size of basis defect states (3), though it would be interesting to estimate $\Delta\mathcal{S}_s$ from an improved lattice gas mapping, as discussed in the end of Sec. IIb, or from the exact-diagonalization data. Propagating n-magnon states can be separated by rather small gaps from n-LM states. Therefore, Eq. (10) describes the slope of the actual transition line $H_c(T)$ in the frustrated quantum antiferromagnet at $T \to 0$.

III. PYROCHLORE ANTIFERROMAGNET

A. Localized magnons

The primitive unit cell of a pyrochlore lattice contains 4 spins belonging to one tetrahedron. These tetrahedra are arranged into an fcc lattice, which is formed by the elementary translations on $\mathbf{a}_1 = (0, 1/2, 1/2)$, $\mathbf{a}_2 = (1/2, 0, 1/2)$, and $\mathbf{a}_3 = (1/2, 1/2, 0)$. (Linear size of the standard cubic cell with 16 spins is chosen as the unit of length.[38]) In a strong magnetic field, where the saturated phase is stable, the four one-magnon excitation branches are given by

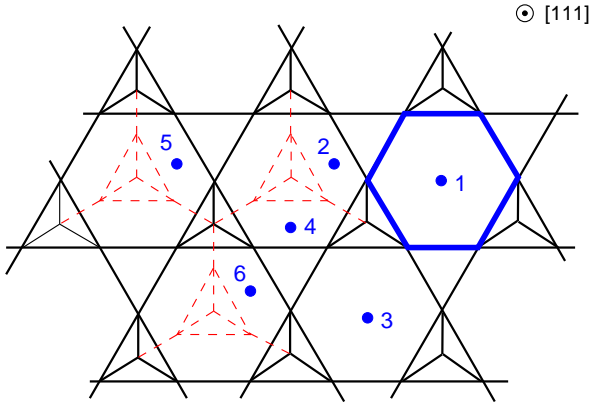$$\omega_{1,2} = H - 8JS, \quad \omega_{3,4} = H - 4JS \pm 2JS\sqrt{1+\eta_{\mathbf{k}}},$$

FIG. 7: (color online). Cross-section of a pyrochlore lattice perpendicular to the [111] axis. Tetrahedra from the same kagomé layer are drawn by solid lines. Thick line shows a localized magnon on one of the hexagons in the kagomé plane. Dashed lines indicate tetrahedra from the upper kagomé layer (shown only partially). Dots with numbers denote centers of hexagons in horizontal and tilted planes, which form a dual pyrochlore lattice.

$$\eta_{\mathbf{k}} = \cos\frac{k_x}{2}\cos\frac{k_y}{2} + \cos\frac{k_y}{2}\cos\frac{k_z}{2} + \cos\frac{k_z}{2}\cos\frac{k_x}{2}. \quad (11)$$

The saturation field of an antiferromagnet on a pyrochlore lattice is the same as for a checkerboard lattice: $H_s = 8JS$. Two dispersionless branches $\omega_{1,2}$ contain $2 \times (N/4 - 1) = N/2 - 2$ linearly independent localized modes, N being the number of pyrochlore lattice sites. Geometric interpretation of these modes is essentially the same as for two-dimensional frustrated lattices. The smallest LMs are located on hexagon voids of kagomé layers, which alternate with triangular layers along the [111] and three other equivalent directions, see Fig. 7. An N-site pyrochlore cluster contains N hexagons, which for $N \to \infty$ is twice more than the number of localized modes in the two lowest branches (11). The 'elementary' hexagon modes are, therefore, not only nonorthogonal but also form an overcomplete basis. This can be explained by observing that hexagon loops on a pyrochlore lattice obey exactly $N/2$ linear relations, which leaves only $N/2$ linearly independent states.[17] Despite this fact we shall use below the hexagon states as a basis in a mapping of a pyrochlore antiferromagnet near H_s on a lattice gas model. Such a representation gives an incorrect (larger) number of states in the magnetization subsectors with nonmacroscopic numbers of LMs. The mapping becomes not so bad for the multi-magnon subsectors in the vicinity of close-packed structures, when the allowed configurations do not include linearly dependent states. In particular, using the lattice gas representation we shall be able to describe an *exact* structure of the magnon crystal for a pyrochlore antiferromagnet.

The lowest-energy multi-particle states are constructed using the same prescription as for two-dimensional frustrated models: LMs are represented by closed even-sites

graphs, which are not directly connected by the exchange bonds. For example, if a LM occupies a hexagon void denoted by 1 in Fig. 7, then no LMs can be placed on hexagons denoted by numbers 2, 3 and 4, since they either share sites with the hexagon 1 or are connected to it by the nearest-neighbor bonds. The lattice gas model is constructed on a dual lattice formed by centers of hexagons of the original pyrochlore lattice, such that an exclusion principle for neighboring sites reproduces the above rules for LMs. Remarkably, the dual lattice is again a pyrochlore lattice. (This explains, in particular, why the number of hexagons is equal to the number of sites.) If the nearest-neighbor distance is denoted by d ($d \equiv \sqrt{2}/4$), then presence of a particle on a given site excludes for occupation (i) 6 nearest-neighbor sites at the distance d as, for example, a pair of sites (hexagons) 2 and 4 in Fig. 7, (ii) 12 second-neighbor sites at the distance $\sqrt{3}d$, e.g., a pair of sites 1 and 2, (iii) 6 third-neighbor sites at the distance $2d$, e.g., sites 1 and 3, and (iv) 12 fourth-neighbor sites at the distance $\sqrt{5}d$, e.g., sites 1 and 4. Note, that on a pyrochlore lattice there are two types of third-neighbor sites at the distance $2d$. The first type used above corresponds to pairs on opposite vertices of hexagons. The second type of third neighbors correspond to pairs with a third site in between. There are again 6 third-neighbor sites of this type around a given site. In terms of the original lattice they correspond to hexagon pairs (2,5) and (2,6) in Fig. 7, which allow simultaneous occupation by LMs. These hexagons belong to two different parallel kagomé planes.

Let us now consider possible magnon crystal states obtained by a close-packing of the smallest LMs on hexagon voids. The initial estimate for the maximal density of LMs has been obtained from the known result for a single kagomé plane:[15] filling one-third of hexagons in every kagomé plane, which is perpendicular to one of the four cubic diagonals, gives $n_0 = (1/3) \times (1/4) = 1/12$ for the density. No arguments were given yet that this is indeed the maximal possible density. In terms of the effective lattice gas model, which operates on a dual pyrochlore lattice, a close-packed structure is constructed by filling every second site in one of the six chains formed by six edges of one tetrahedron, see Fig. 8. Particles at the distance $2d$ along the chains correspond to the second type of third-neighbors and are allowed by the exclusion principle. All chains parallel to a chosen direction form a triangular lattice in the perpendicular plane. Half-filling of the nearest-neighbor chains is prohibited by the exclusion principle, whereas second-neighbor chains in the triangular plane allow for simultaneous occupation. In this way it is possible to put particles only on one-third of the parallel chains, which again yields $n_0 = (1/2) \times (1/3) \times (1/2) = 1/12$ for the particle density. (The last factor $1/2$ corresponds to the fact that parallel chains contain only a half of all lattice sites, the other half belongs to the perpendicular chains.) An example of the constructed structure is shown in Fig. 8. Particles in every chain can be independently shifted by half a pe-
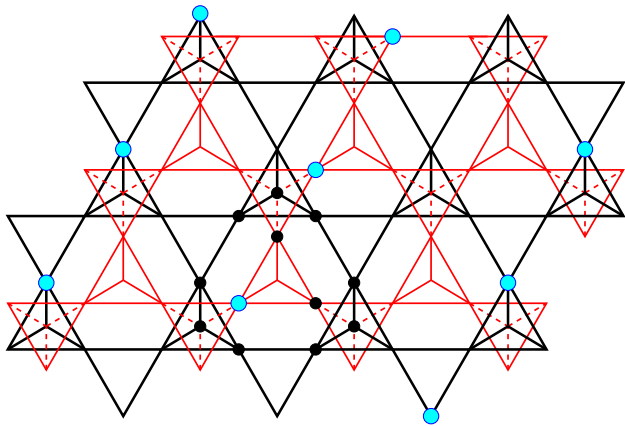
FIG. 8: (color online). Close-packed structure of particles (large light circles) on a dual pyrochlore lattice. Thick (thin) lines represent tetrahedra from the lower (upper) kagomé layer. Small dark circles denote vertices of one truncated tetrahedron.

riod, which corresponds to the degeneracy $N_{\text{deg}} \sim 2^{L^2}$. Once all chains are in phase, *i.e.*, all particles occupy same vertex of the unit cell tetrahedron, we recover the initial structure constructed by filling hexagons in parallel kagomé planes.

To prove that the estimate $n_0 = 1/12$ gives the maximal possible density of localized magnons we consider a polyhedron formed by 4 hexagons and 4 triangles, which has 12 vertices marked by small circles in Fig. 8. This polyhedron is called truncated tetrahedron and belongs to the thirteen Archimedean solids. A special role of this polyhedron for our problem is determined by its geometrical structure: distance between two arbitrary vertices of a truncated tetrahedron is equal to d, $\sqrt{3}d$, $2d$, or $\sqrt{5}d$. If one vertex of a truncated tetrahedron is occupied by a particle, then, according to the above exclusion rules all other vertices must be empty. Simple consideration yields that an N-site pyrochlore lattice contains $N/2$ truncated tetrahedra such that every lattice site is shared between six of them. Counting now becomes straightforward: the number of hard-core particles in the effective lattice-gas model cannot exceed one particle per six truncated tetrahedra $(1/6) \times (N/2)$, which yields $1/12$ as the upper bound on n. Above, we have constructed an explicit example of the particle arrangement with the density $n_0 = 1/12$, therefore, this is indeed the highest density of the close-packed structure.

B. Effective lattice-gas model

Finite-temperature properties of the effective lattice-gas model have been studied by Monte Carlo simulations. In the low-density disordered regime $z < 1$ we use the same annealing protocol as in the 2D case and investigate cubic clusters with periodic boundary condi-

tions and $N = 4L^3$ sites, $L = 6$–12. At $\mu = 0$ ($z = 1$) the entropy obtained by numerical integration of MC data and the density of particles are equal to

$$\mathcal{S}/N = 0.1329(1) \, , \quad n = 0.04718(1) \, , \qquad (12)$$

which yields $M = 1/2 - n \approx 0.4528$ for the magnetization.

In order to study the high-density regime $z > 1$ we employ the exchange MC algorithm with 80 replicas distributed in the range $0 < \ln z < 7$. In contrast with the 2D case we still find significant equilibration problem for large lattices, which exhibit extremely long relaxation times $t \gtrsim 10^7$ MC steps despite of a high exchange rate ~ 0.8 between replicas. Sufficient statistics has been obtained only for three system sizes: two cubic clusters with $L = 4, 6$ and a tetragonal prism with $6 \times 6 \times 12$ unit cells (1728 sites). They were equilibrated for 5×10^5 exchange MC steps and further 10^7 MC steps were used for measurements. Evolution of the particle density with increasing z is presented in Fig. 9 for the two biggest systems. In the vicinity of $\ln z \approx 5.5$ there is an abrupt jump of n to the value, which is very close to the density of the close-packed structure $n_0 = 1/12$.

We expect that the ordered state at $\ln z \gtrsim 5.5$ exhibits only a partial breaking of the translational symmetry. Similar to the studied 2D model, the half-filled chains remain uncorrelated. This tendency should be even more pronounced for the pyrochlore lattice gas in view of an increased entropic effect from disordering determined by a larger N_{deg}. As a result, the symmetry breaking includes only (i) selection of a chain direction and (ii) formation of $\sqrt{3} \times \sqrt{3}$ structure on a triangular lattice in the perpendicular plane. In view of small available system sizes we have not performed investigation of the corresponding order parameters. Instead we have tried to clarify the nature of a possible phase transition into a close-packed
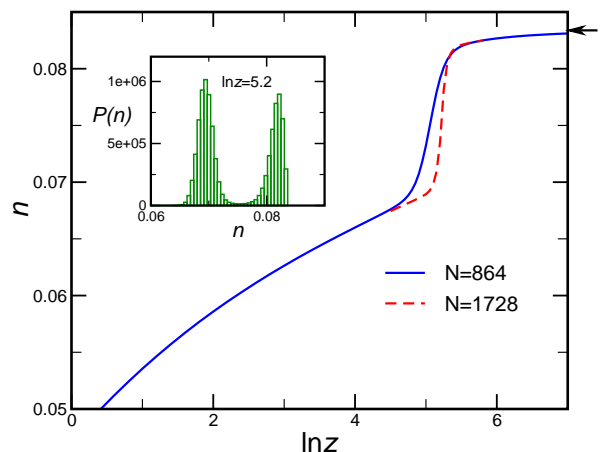

FIG. 9: (color online). Density of a lattice gas on a pyrochlore lattice as a function of $\ln z = \mu/T$. Arrow indicates the density of a close-packed structure $n_0 = 1/12$. Inset: probability distribution for the particle density obtained for $N = 1728$ cluster at $\ln z = 5.2$.

structure by collecting histograms for the particle density. Results for $N = 1728$ lattice at $\ln z = 5.2$ obtained with 10^7 MC steps are presented in the inset of Fig. 9. A clear double peak structure with approximately equal weights in each peak points at a first-order transition. This should be, of course, confirmed by a similar study of larger clusters. We, therefore, put a tentative estimate $\ln z_c = 5.2 \pm 0.2$ for the first-order transition into the magnon crystal state for a pyrochlore antiferromagnet.

Since the original and the dual pyrochlore lattices have the same number of sites, the properties of a spin-1/2 pyrochlore antiferromagnet are obtained from the above results without any rescaling. In particular, the estimate for the entropy at the saturation field is given by Eq. (12). At zero temperature and $H = H_s$ the magnetization jumps from $M = 5/12$ in the plateau region to the full saturation with $M = 1/2$. At finite temperatures the jump in the magnetization is much smaller $\Delta M \approx 0.015$, see Fig. 9. Afterward, $M(H)$ increases smoothly and asymptotically saturates. The first-order transition into the magnon crystal state takes place at

$$H_c(T) = H_s - T \ln z_c \approx 4J - 5.2T \qquad (13)$$

for a spin-1/2 model.

IV. EFFECT OF EXTRA EXCHANGES

In the previous two sections, we have found that the magnon crystal states in checkerboard and pyrochlore antiferromagnets exhibit massive degeneracy at $T = 0$. The degeneracy is not lifted at finite temperatures by fluctuations within the LM subspace. This leads to interesting types of broken symmetries in 2D and 3D cases. In principle, fluctuations to higher energy states outside the LM ensemble at $T > 0$ can favor one or the other type of close-packed magnon structures. Such a scenario cannot be excluded on general grounds. The higher energy states are, however, separated by finite gaps from LMs. Therefore, there must be a region near $T \to 0$, $H \to H_s - 0$, where such a selection is ineffective and only a partial breaking of translational symmetry takes place. Another mechanism of degeneracy lifting can be provided by the magnetoelastic coupling,[39] though the corresponding study has considered only one possible pattern of LMs for each of the two lattices. In the following we investigate the third possibility: effect of further neighbor exchanges,[40] which play significant role in some magnetic materials with pyrochlore lattices.[41,42,43,44,45]

We begin with the checkerboard antiferromagnet, considering an additional weak diagonal exchange of strength J', see Fig. 1b. The magnon crystal state becomes completely unstable at a certain critical value of J'.[10] We are interested in the subcritical regime $|J'| \to 0$. Let us consider two localized magnons (4) on adjacent square plaquettes along the [11] direction: $|\varphi_i\rangle$ and $|\varphi_{i+2\mathbf{a}_1}\rangle$, see Fig. 2 and Sec. IIa for the notations. These LMs are connected by an additional exchange bond

$\hat{V} = J' \mathbf{S}_{2,i} \cdot \mathbf{S}_{4,i+2\mathbf{a}_1}$. To measure energy shifts relative to the energy of the fully polarized state, we shall always subtract a constant from the exchange bond operators: $\hat{V} \to \hat{V} - J'S^2$. The potential energy U of two LMs on adjacent voids is found by calculating the expectation value of $\hat{V}$ over the two-magnon state $|\psi\rangle = |\varphi_i\varphi_{i+2\mathbf{a}_1}\rangle$ and correcting it by the self-energy of LMs without neighbors:

$$U = \langle\psi|\hat{V}|\psi\rangle - 2\langle\varphi_i|\hat{V}|\varphi_i\rangle = J'/16 . \qquad (14)$$

This result applies to an arbitrary spin value S. For $J' > 0$ presence of LMs on adjacent square voids is energetically unfavorable, because two spin flips with a finite probability occupy the same J' bond. Degeneracy of the magnon crystal is, consequently, lifted in favor of an orthorhombic structure: half-filled rows of LMs alternate in phase in order to minimize the contribution (14) between the rows. For $J' < 0$ localized magnons attract each other and the (2×2) tetragonal close-packed structure is stabilized.

The interaction energy between two LMs residing on hexagon voids of pyrochlore lattice is obtained in the same way as Eq. (14) with the result $U = J'/36$. For a pyrochlore antiferromagnet three additional exchanges may be present:[40,45] the second-neighbor exchange J_2 for spin pairs at distance $\sqrt{3}d$, the third-neighbor exchange J_{31} for spin pairs at distance $2d$ on opposite vertices of hexagons, and the third-neighbor exchange J_{32} for spin pairs at distance $2d$ along chains, see Fig. 1a. (Details about the crystal structure of pyrochlore oxides can be found, e.g., in Ref. 38.) Similar to the 2D case the weak additional exchanges select relative shift between adjacent half-filled chains of LMs. If two chains are not shifted relative to each other, LMs occupy hexagons in parallel kagomé planes, whereas if the shift is present, LMs form a nonplanar structure. Analysis of further neighbor exchange links between hexagons on a pyrochlore lattice is straightforward but cumbersome. Below we only summarize the conclusions. Once the two chains of LMs form a planar structure, one LM from the first chain is coupled to two hexagons in the second chain: to a hexagon in the same kagomé plane by two J_2 and two J_{32} bonds and to a hexagon in a parallel kagomé plane by a J_{31} bond. Then, the interaction energy between chains normalized per one LM of the first chain is $U_1 = (2J_2 + J_{31} + 2J_{32})/36$. In the nonplanar structure a given LM from the first chain is coupled to only one non-planar hexagon by three J_2 bonds and one J_{32} bond, which yields $U_2 = (3J_2 + J_{32})/36$.

Comparing the interaction energies U_1 and U_2 for the two structures, we conclude that for $(J_{31} + J_{32} - J_2) < 0$ localized magnons occupy hexagons in parallel kagomé planes. Between the planes LMs follow the ABCABC... structure of close-packed hard spheres. If the above expression changes sign, then LMs form a more complicated nonplanar structure. Amazingly enough, it is again frustrated and degenerate: half-filled chains form a triangular lattice, therefore, antiphase shifts would correspond

to an effective Ising antiferromagnet on a triangular lattice. The residual degeneracy should be finally lifted by zero-point fluctuations induced by the next-neighbor exchanges. The corresponding energy scale is of the order of J'^2/J.

V. SUMMARY

Knowledge of the exact ground state and the single-particle excitation spectrum of frustrated quantum antiferromagnets above the saturation field H_s allows to develop a quantitative description of their thermodynamic properties in a finite range of fields $H \lesssim H_s$ and temperatures $T \to 0$. Localized nature of the lowest energy excitations leads to a mapping onto lattice gas models of hard-core classical particles with an appropriate exclusion principle. As a result, frustrated quantum antiferromagnets preserve a macroscopic degeneracy (finite entropy) at $H = H_s$ and $T = 0$. The close-packed structure of particles (localized magnons) corresponds to the magnon crystal state, which breaks only translational symmetry and preserves continuous rotations about the field direction.

The main finding of our study is high degeneracy of the magnon crystal states in pyroclore and checkerboard antiferromagnets at zero temperature. This, however, does not exclude presence of finite-temperature phase transitions. The corresponding lattice gas models have been studied by the exchange Monte Carlo method. Specifically, we have found numerically the location $\ln z_c = 4.56(2)$ and two critical exponents $\beta = 0.13(1)$ and $\nu = 0.86(2)$ for a square-lattice gas with the second-neighbor exclusion, which describes a checkerboard antiferromagnet. Further numerical work is needed to clarify small differences with the recent independent MC study of the same model.[37] Monte Carlo simulations for the pyroclore-lattice gas show a sharp jump in the particle density, which suggests a first-order transition into a partially ordered crystal phase.

[1] J. Villain, R. Bidaux, J. P. Carton, and R. J. Conte, J. de Phys. **41**, 1263 (1980).

[2] E. F. Shender, Sov. Phys. JETP **56**, 178 (1982).

[3] C. L. Henley, Phys. Rev. Lett. **62** 2056 (1989).

[4] D. S. Rokhsar and S. A. Kivelson, Phys. Rev. Lett. **61**, 2376 (1988).

[5] D. C. Cabra, M. D. Grynberg, P. C. W. Holdsworth, A. Honecker, P. Pujol, J. Richter, D. Schmalfuss, and J. Schulenburg, Phys. Rev. B **71**, 144420 (2005)

[6] M. E. Zhitomirsky, Phys. Rev. B **71**, 214413 (2005).

[7] D. L. Bergman, R. Shindou, G. A. Fiete, and L. Balents, Phys. Rev. Lett. **96**, 097207 (2006).

[8] U. Hizi and C. L. Henley, Phys. Rev. B **73**, 054403 (2006).

[9] M. E. Zhitomirsky and H. Tsunetsugu, Phys. Rev. B **70**, 100403(R) (2004).

[10] M. E. Zhitomirsky and H. Tsunetsugu, Prog. Theor. Phys. Suppl. **160**, 361 (2005).

[11] O. Derzhko and J. Richter, Phys. Rev. B **70**, 104415 (2004).

[12] J. Richter, O. Derzhko, T. Krokhmalskii, Phys. Rev. B **74**, 144430 (2006).

[13] R. J. Baxter, *Exactly Solved Models in Statistical Mechanics* (Academic Press, London, 1982).

[14] J. Schnack, H.-J. Schmidt, J. Richter, and J. Schulenburg, Eur. Phys. J. B **24**, 475 (2001).

[15] J. Schulenburg, A. Honecker, J. Schnack, J. Richter, and H.-J. Schmidt, Phys. Rev. Lett. **88**, 167207 (2002).

[16] H.-J. Schmidt, J. Phys. A **35**, 6545 (2002).

[17] M. E. Zhitomirsky, Phys. Rev. B **67**, 104421 (2003).

[18] J. Richter, J. Schulenburg, A. Honecker, J. Schnack, and H.-J. Schmidt, J. Phys.: Condens. Matter **16**, S779 (2004).

[19] H.-J. Schmidt, J. Richter, and R. Moessner, J. Phys. A **39**, 10673 (2006).

[20] L. K. Runnels, Phys. Rev. Lett. **15**, 581 (1965).

[21] F. H. Ree and D. A. Chestnut, Phys. Rev. Lett. **18**, 5 (1967).

[22] A. Bellemans and R. K. Nigam, J. Chem. Phys. **46**, 2922 (1967).

[23] E. Domany and E. K. Riedel, Phys. Rev. Lett. **40**, 561 (1978).

[24] K. Binder and D. P. Landau, Phys. Rev. B **21**, 1941 (1980).

[25] W. Kinzel and M. Schick, Phys. Rev. B **24**, 324 (1981).

[26] M. Schick, Physica B **109&110**, 1811 (1982).

[27] K. Kaski, W. Kinzel and J. D. Gunton, Phys. Rev. B **27**, 6777 (1983).

[28] R. J. Baxter, Ann. Comb. **3**, 191 (1999).

[29] B. D. Metcalf and C. P. Yang, Phys. Rev. B **18**, 2304 (1978).

[30] Z. Ràcz, Phys. Rev. B **21**, 4012 (1980).

[31] S. Elitzur, R. B. Pearson, and J. Shigemitsu, Phys. Rev. D **19**, 3698 (1979).

[32] P. Ruján, G. O. Williams, H. L. Frisch, and G. Forgács, Phys. Rev. B **23**, 1362 (1981).

[33] F. Y. Wu, Rev. Mod. Phys. **54**, 235 (1982).

[34] J. V. José, L. P. Kadanoff, S. Kirkpatrick, and D. R. Nelson, Phys. Rev. B **16**, 1217 (1977).

[35] K. Hukushima and K. Nemoto, J. Phys. Soc. Jpn. **65**, 1604 (1996).

[36] K. Binder, Z. Phys. B **43**, 119 (1981).

[37] H. C. M. Fernandes, J. J. Arenzon, and Y. Levin,

arXiv:cond-mat/0612372v1.

[38] B. J. Kennedy, B. A. Hunter, and C. J. Howard, J. Solid State Chem. **130**, 58 (1997).

[39] J. Richter, O. Derzhko, and J. Schulenburg, Phys. Rev. Lett. **93**, 107206 (2004); O. Derzhko and J. Richter, Phys. Rev. B **72**, 094437 (2005).

[40] J. N. Reimers, A. J. Berlinsky, and A.-C. Shi, Phys. Rev. B **43**, 865 (1991).

[41] M. K. Crawford, R. L. Harlow, P. L. Lee, Y. Zhang, J. Hormadaly, R. Flippen, Q. Huang, J. W. Lynn, R. Stevens, B. F. Woodfield, J. Boerio-Goates, and R. A. Fisher, Phys.

Rev. B **68**, 220408(R) (2003).

[42] H. Tsunetsugu and Y. Motome, Phys. Rev. B **68**, 060405(R) (2003).

[43] O. Cepas and B. S. Shastry, Phys. Rev. B **69**, 184402 (2004).

[44] Y. Motome and H. Tsunetsugu, Phys. Rev. B **70**, 184427 (2004); Prog. Theor. Phys. Suppl. **160**, 203 (2005).

[45] A. S. Wills, M. E. Zhitomirsky, B. Canals, J. P. Sanchez, P. Bonville, P. Dalmas de Reotier, and A. Yaouanc, J. Phys.: Condens. Matter **18**, L37 (2006).